MULTI-SCALE MODELING OF COMPOSITES WITH RANDOMLY DISTRIBUTED PHASES

Jiří Šejnoha and Michal Šejnoha
Czech Technical University, Faculty of Civil Engineering, Thákurova 7, 166 29 Praha 6
e-mail: sejnoha@fsv.cvut.cz

ABSTRACT
The present contribution introduces an efficient procedure for modeling of nonlinear response of woven composite tubes. It relies on numerical analysis of such a complex composite structure at two different scales (meso and micro-scales). Note that the two analysis steps at individual scales are currently performed independently in the sense that output from one is used as an input to the second. As suggested in the paper, an accurate geometrical description of the tube at both scales is then of paramount importance.

1 INTRODUCTION

It has been recognized long ago that a successful prediction of the macroscopic behavior of complex layered composite structures calls for modeling on various size scales. Multi-scale or hierarchical modeling now offers means to bridge length scale differences ranging from the size scale of microns to large composite structures [3], [4], [10]. In context of the present paper, the large macroscopic structural part is represented by the wound composite tube of Fig. 1(a), while the smallest scale considered herein is of the size of graphite fiber diameter, which is about 10μm.

While the periodic nature of a fiber-tows arrangement, Fig. 1(a), reduces the basic geometrical model on meso scale to a certain periodic unit cell, the distribution of fibers within individual tows (micro-scale) assumes random character, see Fig. 1(c). Analysis of material systems with periodic fields is now well understood and the interested reader may consult work of, e.g., [11], [12] among others. Analyses of material systems with disordered microstructures, however, are still a subject of ongoing research. Some promising directions are discussed in papers [8], [16]. In the present contribution, this difficulty is handled by employing a computational model based on the extended Hashin-Shtrikman variational principles [5], [15] to provide estimates of the local fields on micro-scale.

In contrast with purely elastic behavior commonly assumed for fibers, the matrix phase may undergo nonlinear viscoelastic deformation described by the generalized Leonov model [6]. An algorithm, similar to the fixed point methods, is developed to assess equilibrium at this level. Numerical analysis on micro-scale is then followed by mesoscopic analysis of a certain periodic unit cell. Standard homogenization technique based on periodic fields is implemented within the framework of the finite element method [11], [7]. Standard Newton-Raphson method is called to attain the equilibrium state at meso-level.

The paper is organized as follows. Section 2 reviews computational aspects of the generalized compressive Leonov model. A micromechanical analysis of composite systems with disordered microstructures is discussed in Section 3.1. Section 3.2 then outlines the most important geometrical and numerical aspects of computational modeling on meso-scale. The algorithm for two-step analysis including nonlinear effects is presented in Section 4.

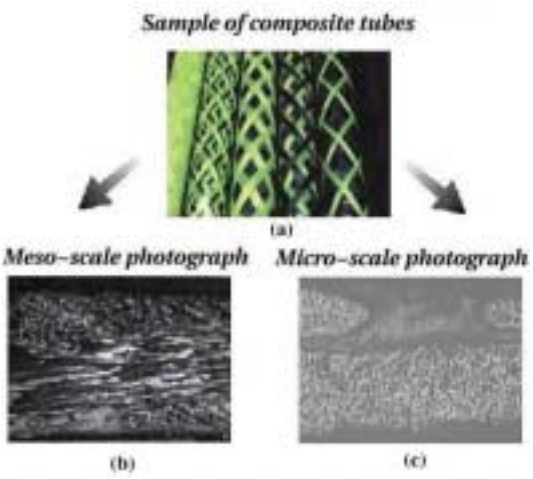

Fig. 1. Multi-scale model

2 MATERIAL MODEL FOR POLYMERS

It is an experimental fact that, to a good approximation, polymers show negligible volume deformation during plastic flow. Combining the Eyring flow model for the plastic component of the shear rate

$$\dot{\gamma}_p = \frac{1}{A}\sinh\frac{\tau}{\tau_0}, \tag{1}$$

with the elastic rate yields the Leonov constitutive 1D model

$$\dot{\gamma} = \dot{\gamma}_e + \frac{\tau}{\eta(\dot{\gamma}_p)}, \tag{2}$$

where

$$\eta(\dot{\gamma}_p) = \eta_0 \frac{\frac{\tau}{\tau_0}}{\sinh\frac{\tau}{\tau_0}} = \eta_0 a_\sigma(\tau). \tag{3}$$

In Eq. (3), η is a stress dependent viscosity, and A, τ_0 are material parameters; a_σ is the shift function and $\eta_0 = A\tau_0$ is referred to as the zero shear viscosity (viscosity, which corresponds to an elastic response). As evident from Eq. (2) the so-called "single Leonov mode" can be represented by the Maxwell model with variable viscosity.

To describe three-dimensional relaxation behavior, a "compressible Leonov mode" can be used and extended to a "multi-mode" formulation, which corresponds to the generalized Maxwell chain model. As shown in [13], the bimodal spectrum of relaxation times of polymer glass requires that individual elements of the Maxwell model be grouped into two sets representing the glass transition and reptation processes, respectively.

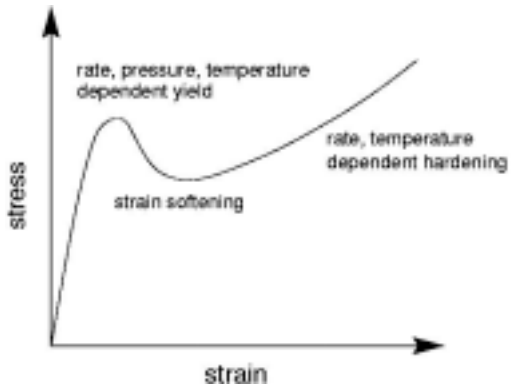

Fig. 2. Stress-strain curve of an amorphous polymer

The nonlinear flow effects arising after the yield point is reached (Fig. 2) can be incorporated into the viscosity parameters of a chain model. For the μ^{th} unit the modified viscosity term assumes the form

$$\eta_\mu = \eta_{0\mu} a_\sigma(\tau_{eq})\, a_\gamma(\dot{\gamma}_{eq}), \tag{4}$$

where

$$\tau_{eq} = \sqrt{\frac{1}{2} s_{ij} s_{ij}}, \qquad \dot{\gamma}_{eq} = \sqrt{2\dot{e}_{ij}^{\,p} \dot{e}_{ij}^{\,p}} \tag{5}$$

are the equivalent shear stress and equivalent plastic shear strain rate, respectively. Tensors s_{ij}, e_{ij} represent the deviatoric parts of the stress and strain tensors. Note that γ_{eq} reduces to pure plastic shear γ_p in 1D. The shift factor a_γ is obtained by integrating the evolution equation

$$\dot{D} = h\left(1 - \frac{D}{D_\infty}\right)\dot{\gamma}_{eq}, \tag{6}$$

along with the expression

$$a_\gamma = \exp(-D). \tag{7}$$

Eqs. (6) and (7) represent a phenomenological description of strain softening using a scalar variable D. Constants D_∞ and h are fitting parameters derived experimentally.

If we limit our attention to the vicinity of the yield point, the kinematic equations for finite deformations can be simplified assuming small strains and a set of constitutive equations of the compressible Leonov model, written in the contracted matrix form, becomes

$$\begin{aligned} \sigma_m &= K\varepsilon_v, \\ \dot{\boldsymbol{s}} &= 2\sum_{\mu=1}^{M} G_\mu \mathbf{Q}\left(\dot{\boldsymbol{e}} - \dot{\boldsymbol{e}}_\mu^{\,p}\right), \\ \dot{\boldsymbol{e}}_\mu^{\,p} &= \mathbf{Q}^{-1}\frac{\boldsymbol{s}_\mu}{2\eta_\mu}, \end{aligned} \tag{8}$$

where K is the bulk modulus, G_μ is the shear modulus of the k^{th} unit, σ_m is the mean stress and ε_v is the volumetric strain. Constants $\eta_{0\mu}$, G_μ, $\mu = 1, \ldots, M$ are found from linear relaxation data.

A simple finite difference based integration scheme can be devised to integrate Eqs. (8). To proceeding, first subdivide the time axis into intervals of length Δt. Next, suppose that at the beginning of the i^{th} interval $< t_{i-1}, t_i >$, the stress vector $\boldsymbol{s}_\mu(\mathbf{x}, t_{i-1})$, $\mu = 1, \ldots, M$, is known. Further assume that functions $\eta_\mu(\mathbf{x}, t) = \eta_\mu(\mathbf{x}, t_i - \Delta t/2)$ remain constant within a given time interval. Then, integrating Eqs. (8) with respect to time over Δt and using

$$\boldsymbol{s}(\mathbf{x},t) = \sum_{\mu=1}^{M} \boldsymbol{s}_\mu(\mathbf{x},t), \tag{9}$$

we arrive after some manipulations at the following incremental form of the local constitutive equation

$$\Delta\boldsymbol{\sigma}_i(\mathbf{x}) = \hat{\mathbf{L}}_i(\mathbf{x})\Delta\boldsymbol{\varepsilon}_i(\mathbf{x}) + \Delta\hat{\boldsymbol{\sigma}}_i(\mathbf{x}), \tag{10}$$

where

$$\hat{\mathbf{L}}_i = \begin{bmatrix} K+\frac{4}{3}\hat{G} & K-\frac{2}{3}\hat{G} & K-\frac{2}{3}\hat{G} & 0 & 0 & 0 \\ K-\frac{2}{3}\hat{G} & K+\frac{4}{3}\hat{G} & K-\frac{2}{3}\hat{G} & 0 & 0 & 0 \\ K-\frac{2}{3}\hat{G} & K-\frac{2}{3}\hat{G} & K+\frac{4}{3}\hat{G} & 0 & 0 & 0 \\ 0 & 0 & 0 & \hat{G} & 0 & 0 \\ 0 & 0 & 0 & 0 & \hat{G} & 0 \\ 0 & 0 & 0 & 0 & 0 & \hat{G} \end{bmatrix}_i, \tag{11}$$

$$\Delta\hat{\boldsymbol{\sigma}}_i = -2\hat{G}_i\,\mathbf{Q}\,\Delta\hat{\boldsymbol{e}}_i, \tag{12}$$

$$\mathbf{Q} = \mathrm{diag}\left[1,1,1,\frac{1}{2},\frac{1}{2},\frac{1}{2}\right]. \tag{13}$$

The time dependent variables are

$$\hat{G}_i = \sum_{\mu=1}^{M} \frac{\eta_{\mu i}}{\Delta t}\left[1-\exp\left(-\frac{G_\mu \Delta t}{\eta_{\mu i}}\right)\right], \tag{14}$$

$$\Delta\hat{\boldsymbol{e}}_i = \frac{1}{2\hat{G}_i}\sum_{\mu=1}^{M}\left[1-\exp\left(-\frac{G_\mu \Delta t}{\eta_{\mu i}}\right)\right]\mathbf{Q}^{-1}\,\boldsymbol{s}_\mu(t_{i-1}), \tag{15}$$

$$\boldsymbol{s}_\mu(t_i) = \boldsymbol{s}_\mu(t_{i-1})\exp\left(\frac{G_\mu \Delta t}{\eta_{\mu i}}\right) + \frac{2\eta_{\mu i}}{\Delta t}\left[1-\exp\left(-\frac{G_\mu \Delta t}{\eta_{\mu i}}\right)\right]\mathbf{Q}\,\Delta\boldsymbol{e}_i. \tag{16}$$

Note that variables in Eqs. (13) - (15) are functions of the deviatoric stress found at time instant t_i. The stress update of Eq. (15) thus requires iterations within each time step. To that end, one may apply an efficient and robust procedure of the fixed-point type. At each load or time increment a first estimation of the stress dependent viscosity is obtained from the stresses found at the beginning of the time step (at time t_{i-1}). Successive iteration is then carried out with viscosity update until two successive solutions for $\boldsymbol{s}(t_i)$ differ by less than a fixed tolerance.

3 TWO-SCALE MODELING OF WOUND COMPOSITE TUBES

Suppose that the composite tube is subjected to macroscopic loading conditions which generate uniform fields throughout individual plies. In such a case the general, three level analysis, simplifies considerably as only the mesoscopic and microscopic response is relevant. Note that the effective fields found on meso-scale correspond to macroscopic ones. Modeling on individual scales is outlined in the following sections.

3.1 Modeling on micro-scale

Here, the investigation is focused on modeling issues pertinent to random, non-periodic systems such as the one depicted in Fig. 1(c). Note that both proper geometrical characterizations of the material system, suitable constitutive

model, and reliable and efficient numerical technique are equally important when developing a computational model on this level of sophistication.

Geometrical model on micro-scale

Consider an ergodic heterogeneous material system with statistically homogeneous distribution of reinforcements. We limit our attention to two-phase fibrous composites with fibers aligned along the x'_3 direction (Fig. 5(b)). The random morphology of such a system, evident from Fig. 1(c), can be conveniently described by the volume fractions of individual phases and the two-point probability function S_{rs} [1], [2]. The matrix-matrix probability function S_{mm} is displayed in Fig. 3. It is worthwhile to mention that only the Fourier transform of function S_{rs} is needed in the subsequent numerical formulation. The details of derivation of required functions can be found in [9], [16], [14].

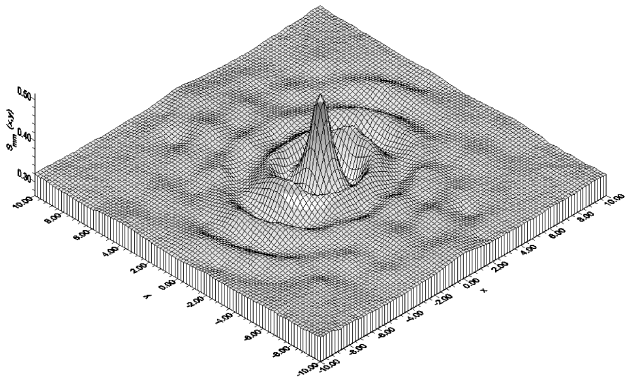

Fig. 3. Two-point probability function $S_{mm}(x_1, x_2)$

Numerical model on micro-scale

As suggested in [14], an efficient and reliable solution procedure for evaluation of both local and overall response of a tow F (a bundle of fibers f, Fig. 1(c)) on micro-scale can be developed on the basis of Hashin-Shtrikman variational principles for elastic media. With reference to combined meso-micro analysis we consider only the primary principle and write the two equivalent representations of local stresses in the form

$$\boldsymbol{\sigma}(\mathbf{x}) = \mathbf{L}(\mathbf{x})\boldsymbol{\varepsilon}(\mathbf{x}) + \boldsymbol{\lambda}(\mathbf{x}) \quad , \qquad \boldsymbol{\sigma}(\mathbf{x}) = \mathbf{L}_0\boldsymbol{\varepsilon}(\mathbf{x}) + \boldsymbol{\tau}(\mathbf{x}), \tag{16}$$

where $\mathbf{L}(\mathbf{x})$ is the local stiffness matrix and $\mathbf{L}_0$ is the stiffness matrix of a certain homogeneous reference medium. Recall that the Hashin-Shtrikman functional reads

$$U_\tau = \frac{1}{2}\int_{\Omega_F} \left(\boldsymbol{E}^{\mathrm{T}}\boldsymbol{\Sigma} - (\boldsymbol{\tau}-\boldsymbol{\lambda})^{\mathrm{T}}(\mathbf{L}-\mathbf{L}_0)^{-1}(\boldsymbol{\tau}-\boldsymbol{\lambda}) - 2\boldsymbol{\tau}^{\mathrm{T}}\boldsymbol{E} + \boldsymbol{\varepsilon}'^{\mathrm{T}}\boldsymbol{\tau} + \boldsymbol{\lambda}^{\mathrm{T}}\mathbf{L}^{-1}\boldsymbol{\lambda} \right) \mathrm{d}\Omega, \tag{17}$$

where $\boldsymbol{E}$ and $\boldsymbol{\Sigma}$ are the overall strains and stresses supplied to the medium from the analysis on meso-scale. The fluctuation part $\boldsymbol{\varepsilon}'$ of the local strain $\boldsymbol{\varepsilon}$ is provided by (see [15])

$$\boldsymbol{\varepsilon}'(\mathbf{x}) = \boldsymbol{\varepsilon}(\mathbf{x}) - \boldsymbol{E} \ . \tag{18}$$

To facilitate the solution we further restrict our attention to a piecewise uniform distribution of polarization stress $\boldsymbol{\tau}_r(\mathbf{x}) = \boldsymbol{\tau}_r$ and the eigenstress vector $\boldsymbol{\lambda}_r(\mathbf{x}) = \boldsymbol{\lambda}_r$ within a given phase $r = f, m$ (fiber, matrix). Taking an ensemble average of functional (17) and performing its variation with respect to $\boldsymbol{\tau}_r$ finally supplies a set of algebraic equations for unknown phase averages of polarization stress $\boldsymbol{\tau}_r$

$$\sum_{s=1}^{n} \left[\delta_{rs}(\mathbf{L}_r - \mathbf{L}_0)^{-1} c_r - \mathbf{A}_{rs} \right] \boldsymbol{\tau}_s = \boldsymbol{E} c_r + (\mathbf{L}_r - \mathbf{L}_0)^{-1} \boldsymbol{\lambda}_r c_r \ , \qquad r = 1, \cdots, n, \tag{19}$$

where the microstructure-dependent matrices $\mathbf{A}_{rs}$ are provided by, see [16]

$$\boldsymbol{A}_{rs} = \int_{\Omega_F} \boldsymbol{\varepsilon}_0^*(\mathbf{x}-\mathbf{x}') \left[S_{rs}(\mathbf{x}-\mathbf{x}') - c_r c_s \right] \mathrm{d}\Omega(\mathbf{x}') = \frac{1}{(2\pi)^2} \int_{\Omega_F} \widetilde{\boldsymbol{\varepsilon}}_0^*(\boldsymbol{\xi}') \widetilde{S}'_{rs}(\boldsymbol{\xi}') \, \mathrm{d}\Omega(\boldsymbol{\xi}'), \tag{20}$$

Symbol ($\tilde{\cdot}$) in Eq. (20) represents the Fourier transform and $\boldsymbol{\varepsilon}_0^*$ is the fundamental solution that relates an initial stress vector $\boldsymbol{\tau}$ applied to a homogeneous and isotropic medium to a strain derived under zero displacement boundary conditions and for which the stress is self-equilibrated. Formal inversion of Eq. (19) yields the mesoscopic constitutive equation for a tow F

$$\boldsymbol{\sigma}_{meso} = \mathbf{L}_{meso}\boldsymbol{\varepsilon}_{meso} + \boldsymbol{\lambda}_{meso}\,, \tag{21}$$

where $\boldsymbol{\varepsilon}_{meso} = \boldsymbol{E}$. The spatially averaged overall stiffness matrix $\mathbf{L}_{meso}$ and the macroscopic eigenstress vector $\boldsymbol{\lambda}_{meso}$ are provided by

$$\mathbf{L}_{meso} = \mathbf{L}_0 + \sum_{r=1}^{n}\sum_{s=1}^{n} c_r \mathbf{T}_{rs} c_s\,, \tag{22}$$

$$\boldsymbol{\lambda}_{meso} = \sum_{r=1}^{n}\sum_{s=1}^{n} c_r \mathbf{T}_{rs} c_s \left(\mathbf{L}_s - \mathbf{L}_0\right)^{-1} \boldsymbol{\lambda}_s\,. \tag{23}$$

$\mathbf{T}_{rs}$ then represent individual blocks of the inverse matrix to the left hand side of system (19).

To introduce the nonlinear effects in the matrix phase we recall Eq. (10). Then, incremental form of Eq. (21) for a tow F becomes

$$\Delta\boldsymbol{\sigma}_{meso,i} = \mathbf{L}_{meso,i}\Delta\boldsymbol{\varepsilon}_{meso,i} + \Delta\boldsymbol{\lambda}_{meso,i}\,. \tag{24}$$

The current increment of $\boldsymbol{\lambda}_{meso}$ and the instantaneous stiffness matrix $\mathbf{L}_m$ of the matrix phase attain the forms

$$\Delta\boldsymbol{\lambda}_{meso,i} = \sum_{r=1}^{n}\sum_{s=1}^{n} c_r \mathbf{T}_{rs} c_s \left(\mathbf{L}_s - \mathbf{L}_0\right)_i^{-1} \Delta\hat{\boldsymbol{\sigma}}_i\,, \quad s = m \rightarrow \mathbf{L}_{m,i} = \hat{\mathbf{L}}_i\,, \tag{25}$$

whereas the fiber phase is assumed elastic. Note that Eq. (10) also applies to the matrix layers bonding the tows (Section 3.2).

3.2 Modeling on meso-scale

As already suggested in the introductory part, the computational modeling on meso-scale reduces to the analysis of a certain periodic unit cell. When subjected to uniform loading and suitable periodic boundary conditions, the homogenized unit cells can be periodically extended to map the inelastic response over the macroscopic domain under consideration.

Geometrical model on meso-scale

For modeling purposes we limit our attention to a two-ply composite tube. Depending on winding speed and orientation the number of tows within periodically repeating regions may vary. In our particular case, the meso-scale unit cell consists of two plies where each ply contains six tows. The tow is formed by unidirectional graphite fibers (approximately 12000 fibers within a tow) bonded to the polymer matrix. Overall properties of this mixture are found from homogenization procedure carried out on the micro-scale. All six tows are aligned along the same direction, but they run through individual plies thus creating a typical woven structure of the composite. This is shown schematically in Fig. 4.

Fig. 4. Weave lay-up

The shape of the tow is derived from images of the real composite structure. One typical cut-out is displayed in Fig. 5(a) showing a portion of the tow cross-section together with longitudinal variation of the tow middle curve. With the help of the LUCIE image analyzer such a micrograph can be transformed into a binary image and further analyzed to provide all geometrical parameters, which are necessary to build an idealized geometrical model such as the one shown in Fig. 5(b).

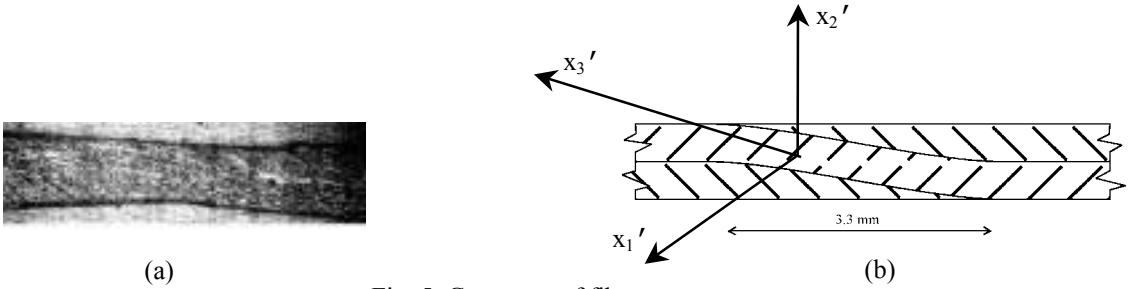

(a) (b)

Fig. 5. Geometry of fiber tow

The microscopic images of a real tube suggest that every tow is impregnated by the polymer matrix, the thickness of which is about 0,03 mm. The interface layer between the two tows is approximately 0,02 mm thick. The same thickness is considered between the two tows, which are parallel to each other and lay in the same ply. To simplify the geometrical model it is contemplated that the shape of the tow cross-section is kept constant along the whole tow. The tow itself is created by translating the tow cross-section along the middle-curve, recall Fig. 5(a). A section of the resulting unit cell generated using the above assumptions appears in Fig. 6(a).

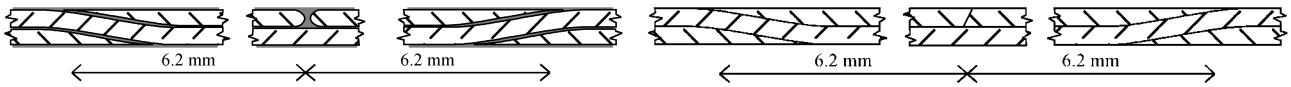

(a) (b)

Fig. 6. Geometrical model of the unit cell – idealization

Such a geometrical model, however, is not very suitable for computational modeling using the finite element method. The main drawback is a very thin interface layer. Its discretization results in very small elements spread over large region of the unit cell thus leading to enormous computational effort, but not substantially increasing the accuracy of the numerical model. Therefore, in order to arrive at a feasible numerical model, some action must be taken. A suitable method of attack appears in replacing the interface layer by contact elements with zero thickness and appropriate interfacial material properties. A section of such a model is depicted in Fig. 6(b).

Numerical model on meso-scale

The section now proceeds by considering a RVE given in terms of the unit cell of Fig. 4. Local coordinate systems with the x_3' axis aligned with the fiber direction is plotted in Fig. 5(b).

Further suppose that the prescribed loading conditions produce a uniform distribution of macroscopic strain field, $\boldsymbol{\varepsilon}_{mac} = \boldsymbol{E}$, or stress field, $\boldsymbol{\sigma}_{mac} = \boldsymbol{\Sigma}$. In either case, an increment of the local displacement field $\boldsymbol{u}_{meso}(\mathbf{x})$ on meso-scale admits the following decomposition (hereafter, subscript i introduced in Eq. (10) is omitted for brevity)

$$\Delta \boldsymbol{u}_{meso}(\mathbf{x}) = \Delta \boldsymbol{E}\mathbf{x} + \Delta \boldsymbol{u}^{*}_{meso}(\mathbf{x}), \tag{26}$$

where $\Delta \boldsymbol{u}^{*}_{meso}(\mathbf{x})$ represents a fluctuation of the local displacement due to the presence of heterogeneities and is considered being periodic, [1], [7], [and reference therein]. The local strain increment then assumes the form

$$\Delta \boldsymbol{\varepsilon}_{meso}(\mathbf{x}) = \Delta \boldsymbol{E} + \Delta \boldsymbol{\varepsilon}^{*}_{meso}(\mathbf{x}), \tag{27}$$

where the fluctuation part $\Delta \boldsymbol{\varepsilon}^{*}_{meso}(\mathbf{x})$ must vanish upon volume averaging. This requirement is fulfilled for the present boundary conditions since

$$\left\langle \Delta \varepsilon^{*}_{ij,meso}(\mathbf{x}) \right\rangle = \frac{1}{\Omega}\int_{\Omega} \Delta \varepsilon^{*}_{ij,meso}(\mathbf{x})\mathrm{d}\Omega = \frac{1}{2\Omega}\int_{\partial\Omega} \left(\Delta u^{*}_{i,meso}(\mathbf{x}) n_j + \Delta u^{*}_{j,meso}(\mathbf{x}) n_i \right) \mathrm{d}(\partial\Omega) = \mathbf{0}, \tag{28}$$

due to periodicity of $\Delta \boldsymbol{u}^{*}_{meso}(\mathbf{x})$ (the same displacement on opposite sides of the unit cell). In Eq. (28) Ω and $\partial\Omega$ now represent the volume and the boundary of the mesoscopic unit cell, respectively.

The goal now becomes the evaluation of local fields within the mesoscopic unit cell and then their averaging to arrive at the desired mesoscopic response. To proceed, we first write the principle of virtual work (Hill's lemma) in the form

(29) $$\left\langle \delta\boldsymbol{\varepsilon}_{meso}^{\mathrm{T}} \Delta\boldsymbol{\sigma}_{meso} \right\rangle = \delta\boldsymbol{E}^{\mathrm{T}} \Delta\boldsymbol{\Sigma} = \left\langle \delta\boldsymbol{\varepsilon}_{meso}^{*\ \mathrm{T}} \Delta\boldsymbol{\sigma} \right\rangle + \delta\boldsymbol{E}^{\mathrm{T}} \left\langle \Delta\boldsymbol{\sigma}_{meso} \right\rangle = \left\langle \delta\boldsymbol{\varepsilon}_{meso}^{*l\ \mathrm{T}} \Delta\boldsymbol{\sigma}_{meso}^{l} \right\rangle + \delta\boldsymbol{E}^{l\mathrm{T}} \left\langle \Delta\boldsymbol{\sigma}_{meso}^{l} \right\rangle ,$$

where upperscript l represents quantities given in the local coordinate system. The local stress increment written in the local coordinate system then reads

(30) $$\Delta\boldsymbol{\sigma}_{meso}^{l}(\mathbf{x}) = \mathbf{L}_{meso}(\mathbf{x})\left(\Delta\boldsymbol{\varepsilon}_{meso}^{*l}(\mathbf{x}) + \Delta\boldsymbol{E}^{l}\right) + \Delta\boldsymbol{\lambda}_{meso}^{l}(\mathbf{x}).$$

When prescribing the overall stress vector $\Delta\boldsymbol{\Sigma}$, Eq. (29) represents a set of equilibrium equations for unknown components of fluctuation part of both the local strain $\Delta\boldsymbol{\varepsilon}_{meso}^{*}$ and uniform macroscopic strain $\boldsymbol{E}$. In the finite element modeling framework Eq. (30) attains the form

(31) $$\Delta\boldsymbol{\sigma}_{meso}^{l}(\mathbf{x}) = \mathbf{L}_{meso}(\mathbf{x})\mathbf{B}(\mathbf{x})\mathbf{T}\Delta\boldsymbol{r}^{g} + \mathbf{L}_{meso}(\mathbf{x})\hat{\mathbf{T}}\Delta\boldsymbol{E} + \Delta\boldsymbol{\lambda}_{meso}^{l}(\boldsymbol{x}),$$

where $\mathbf{B}$ is the strain matrix, $\mathbf{T}$ and $\hat{\mathbf{T}}$ are certain transformation matrices and $\Delta\boldsymbol{r}^{g}$ is the vector of nodal values of the fluctuation part of the displacement field $\Delta\boldsymbol{u}_{meso}^{*}$ in the global coordinate system. Introducing matrix $\hat{\mathbf{B}} = \mathbf{BT}$ and then substituting Eq. (31) into Eq. (29) provides the discretized form of the governing equations as

(32) $$\begin{bmatrix} \frac{1}{\Omega}\int_{\Omega} \hat{\mathbf{T}}\mathbf{L}_{meso}(t)\hat{\mathbf{T}}\,\mathrm{d}\Omega & \frac{1}{\Omega}\int_{\Omega} \hat{\mathbf{T}}^{\mathrm{T}}\mathbf{L}_{meso}(t)\hat{\mathbf{B}}\,\mathrm{d}\Omega \\ \frac{1}{\Omega}\int_{\Omega} \hat{\mathbf{B}}^{\mathrm{T}}\mathbf{L}_{meso}(t)\hat{\mathbf{T}}\,\mathrm{d}\Omega & \frac{1}{\Omega}\int_{\Omega} \hat{\mathbf{B}}^{\mathrm{T}}\mathbf{L}_{meso}(t)\hat{\mathbf{B}}\,\mathrm{d}\Omega \end{bmatrix} \begin{Bmatrix} \Delta\boldsymbol{E} \\ \Delta\boldsymbol{r}^{g} \end{Bmatrix} = \begin{Bmatrix} \Delta\boldsymbol{\Sigma} - \frac{1}{\Omega}\int_{\Omega} \hat{\mathbf{T}}\Delta\boldsymbol{\lambda}_{meso}^{l}\,\mathrm{d}\Omega \\ -\frac{1}{\Omega}\int_{\Omega} \hat{\mathbf{B}}^{\mathrm{T}}\Delta\boldsymbol{\lambda}_{meso}^{l}\,\mathrm{d}\Omega \end{Bmatrix}.$$

On the other hand, when prescribing the overall strain vector $\Delta\boldsymbol{E}$, the system of equations (32) reduces to

(33) $$\mathbf{K}(t)\Delta\boldsymbol{r}^{g} = \Delta\mathbf{R},$$

where

(34) $$\mathbf{K}(t) = \frac{1}{\Omega}\int_{\Omega} \hat{\mathbf{B}}^{\mathrm{T}}\mathbf{L}_{meso}(t)\hat{\mathbf{B}}\,\mathrm{d}\Omega,$$

(35) $$\Delta\mathbf{R} = -\frac{1}{\Omega}\int_{\Omega} \hat{\mathbf{B}}^{\mathrm{T}}\mathbf{L}_{meso}(t)\hat{\mathbf{T}}\,\mathrm{d}\Omega\Delta\boldsymbol{E} - \frac{1}{\Omega}\int_{\Omega} \hat{\mathbf{B}}^{\mathrm{T}}\Delta\boldsymbol{\lambda}_{meso}^{l}\,\mathrm{d}\Omega.$$

The following algorithm describes implementation of the proposed two-step multi-scale analysis with reference to nonlinear viscoelastic response of the composite system. Only the prescribed strain conditions, Eq. (33), which are more useful in conjunction with the finite element method, will be considered.

4 MODEL IMPLEMENTATION

Due to limited extent of this paper we give only a rough description of the micro-meso iteration algorithm. Consider a given macroscopic strain vector $\Delta\boldsymbol{E}$. Assume that all the state variables are known at the beginning of the time interval $(t, t + \Delta t)$. The increment $\Delta\boldsymbol{r}^{g}$ is required to satisfied equilibrium at time $t + \Delta t$, that is

(36) $$\left\langle \delta\boldsymbol{\varepsilon}^{*\mathrm{T}} \boldsymbol{\sigma}_{meso} \right\rangle = 0,$$

where $\Delta\boldsymbol{\sigma}_{meso}^{*}(t+\Delta t)$ depends on $\Delta\boldsymbol{\sigma}_{meso}^{*}(t)$ and on the increments $\Delta\boldsymbol{r}^{g}$ and $\Delta\boldsymbol{E}$. Therefore, Eq. (36) is nonlinear and iterative scheme must be used within each time interval. Denote the k^{th} iteration step by the upperscript k and update

(37) $$^{k+1}\Delta\boldsymbol{r}^{g} = {}^{k}\Delta\boldsymbol{r}^{g} + {}^{k+1}\delta\boldsymbol{r}^{g},$$

(38) $$^{k+1}\boldsymbol{\sigma}_{meso} = {}^{k}\Delta\boldsymbol{\sigma}_{meso} + {}^{k+1}\delta\boldsymbol{\sigma}_{meso}.$$

Combining Eqs. (36)-(38) yields, [7],

(39) $$\int_{\Omega} \hat{\mathbf{B}}^{\mathrm{T}} \left({}^{k}\boldsymbol{\sigma}_{meso} + \mathbf{L}_{meso} \hat{\mathbf{B}}^{k+1} \delta \boldsymbol{r}^{g} \right) \mathrm{d}\Omega = 0 .$$

The desired increment of the displacement ${}^{k+1}\delta \boldsymbol{r}^{g}$ is then found from

(40) $$\mathbf{K}^{k+1} \delta \boldsymbol{r}^{g} = -\int_{\Omega} \hat{\mathbf{B}}^{\mathrm{T}^{k}} \boldsymbol{\sigma}_{meso} \, \mathrm{d}\Omega .$$

The tangential stiffness matrix **K** is taken from the beginning of the time interval and kept constant during iteration. The current mesoscopic stress is calculated by means of material Eqs. (10)-(15) together with (25) and (24). The stress update procedure carried out on micro-scale is discussed in Section 2.

Acknowledgment
This work was sponsored by the GAČR grants 103/00/0756 and GP103/01/D052.

REFERENCES

[1] Beran, M. J. Statistical Continuum Theories, Monographs in Statistical Physics, Interscience Publishers, 1968.
[2] Drugan, W. J. and Willis, J. R. A micromechanics-based nonlocal constitutive equation and estimates of representative volume element size for elastic composites. *Journal of the Mechanics and Physics of Solids*, **44** (1996), No. 4, 497-524.
[3] Fish, J. and Shek, K. Multiscale analysis of large-scale nonlinear structures and materials. *Int. Journal for Computational Civil and Structural Engineering*, **1** (2000), No. 1, 79-90.
[4] Fish, J., Shek, K., Pandheeradi, M., and Shepard, M. Computational plasticity for composite structures based on mathematical homogenization: Theory and practice. *Computer Methods in Applied Mechanics and Engineering*, **148** (1997), 53-73.
[5] Hashin, Z. and Shtrikman, S. A variational approach to the theory of elastic behavior of multiphase materials. *Journal of the Mechanics and Physics of Solids*, **11** (1963), 127-140.
[6] Leonov, A. I. Non-equilibrium thermodynamics and rheology of viscoelastic polymer media. *Rheol. Acta*, **15** (1976), 85-98.
[7] Michel, J. C., Moulinec, H. and Suquet, P. Effective properties of composite materials with periodic microstructure: A computational approach. *Computer Methods in Applied Mechanics and Engineering*, **172** (1999), 109-143.
[8] Povirk, G. L. Incorporation of microstructural information into models of two-phase materials. *Acta metall. mater*., **43** (1995), No. 8, 3199-3206.
[9] Sejnoha, M. Micromechanical Analysis of Random Composites, Habilitation thesis, Czech Technical University in Prague, 2000.
[10] Sejnoha, M. and Sejnoha, J. Multiscale modeling in engineering. *Slovak Journal of Civil Engineering*, in print (2001).
[11] Suquet, P. Elements of homogenization for inelastic solid mechanics, Homogenization Techniques for Composite Media, *Lecture notes in physics*, (Eds. E. Sanchez-Palencia and A. Zaoui), Springer-Verlag, Berlin, **272** (1987), 194-278.
[12] Teplý, J. L. and Dvořák, G. J. Bound on overall instantaneous properties of elastic-plastic composites. *Journal of the Mechanics and Physics of Solids*, **36** (1988), No. 1, 29-58.
[13] Tervoort, T. A. Constitutive modeling of polymer glasses: Finite, nonlinear visocelastic behaviour of polycarbonate. PhD. Thesis, Eindhoven University of Technology, Eindhoven, 1996.
[14] Šejnoha, M. and Zeman, J. Overall viscoelastic response of random fibrous composites with statistically uniform distribution of reinforcements. *Computer methods in applied mechanics and engineering.* Submitted for publication.
[15] Willis, J. R. Bounds and self-consistent estimates for the overall properties of anisotropic composites. *Journal of the Mechanics and Physics of Solids*, **25** (1977), 185-202.
[16] Zeman, J. and Šejnoha, M. Effective properties of graphite fiber tow impregnated by polymer matrix. *Journal of the Mechanics and Physics of Solids*, **49** (2001), 69-90.